J Mater Sci (2011) 46:500–508
DOI 10.1007/s10853-010-4953-y

Phase constituents and thermal expansion behavior of a NiCrAlYRe coating alloy

J. J. Liang · H. Wei · Y. L. Zhu · X. F. Sun · Z. Q. Hu · M. S. Dargusch · X. Yao

Received: 27 April 2010 / Accepted: 24 September 2010 / Published online: 7 October 2010

Abstract Phase constituents and properties of MCrAlY coating alloys play a crucial role in determining the performance of MCrAlY stand-alone overlay coatings and thermal barrier coating systems. Recent advances in computer modeling including access to involved thermodynamic databases make it possible to predict phase stabilities in these alloy systems. This article investigates the phase stabilities of a NiCrAlY coating alloy containing Re both experimentally and thermodynamically. The addition of Re promotes the formation of the Cr-rich α-phase that owns low coefficient of thermal expansion (CTE), and thereby decreases the CTE of the NiCrAlYRe coating alloy. In addition, the martensitic transformation of the B2 β-NiAl phase is investigated. This transformation has an important influence on the microhardness of the β-NiAl phase.

Introduction

The service temperature of gas-turbine blades can currently reach 1150 °C or higher. At such high temperatures, the oxidation behavior of superalloys becomes one of the major life-limiting factors. To overcome this high temperature oxidation problem, many kinds of coatings are applied to the blade surface; an important one of these coatings is the MCrAlY (with M = Co, Ni or combination thereof) coating which can serve as an overlay coatings or as bond coats in thermal barrier coating (TBC) systems [1].

MCrAlY coatings consist mainly of β-NiAl and γ-Ni phases. During service, the phase constituent of the coatings experiences many changes, which have an important influence on the mechanical and physical properties of the coatings [2]. It was reported that a martensitic transformation [3–7] might occur in the β-NiAl phase with more than 63 at.% Ni when quenching from temperatures above 1000 °C. Because the molar volume of the B2 β-NiAl phase is approximately 2% greater than that of $L1_0$ martensite, this transformation will produce about 0.7% linear transformation strain in NiAl coatings [8–10]. Mendis and Hemker [11] estimated that strain induced by the martensitic transformation in a NiCoCrAlY bond coat was about 1.3%. Additionally, the formation of γ'-Ni_3Al [12], α-Cr [13] and σ-phases [14, 15] were observed in MCrAlY coatings after prolonged thermal exposure. The study of Achar et al. [16, 17] revealed that γ'-Ni_3Al in MCrAlY alloys was not an equilibrium phase at high temperatures, and the dissolution of γ'-Ni_3Al would usually give rise to a volume change in a manner similar to martensitic transformation in Pt-modified NiAl bond coats. Mendis and Hemker [11] thought that this effect was very slight in NiCoCrAlY bond coats due to the coherent nature of the interface of γ'-Ni_3Al with the γ-Ni matrix.

With the development of computational thermodynamics, it is possible to give some insights into the phase stabilities through thermodynamic calculations in additions to experimental observations [18]. A major prerequisite for thermodynamic calculations is a reliable description of the thermodynamic parameters for the systems to be studied.

J. J. Liang (✉) · H. Wei · Y. L. Zhu · X. F. Sun · Z. Q. Hu
Institute of Metal Research, CAS, Shenyang 110016, China
e-mail: jjliang@imr.ac.cn

J. J. Liang
Graduate School of Chinese Academy of Sciences (CAS), Beijing 100039, China

H. Wei · M. S. Dargusch · X. Yao
School of Engineering, The University of Queensland, Brisbane, QLD 4072, Australia

Fortunately, ThermoTech Ltd. has offered a thermodynamic database suitable for Ni-base superalloys (TTNi7 database), and Huang and Chang [19–22] and Dupin et al. [23, 24] have developed their own databases for Ni–Al, Ni–Al–Cr, Ni–Cr–Re, and Ni–Al–Cr–Re systems based on thermodynamic assessment of various types of experimental data. It is worth noting that these available thermodynamic databases are mostly assessed on the basis of experimental results obtained from binary and ternary systems. For higher order systems, thermodynamic descriptions are obtained by extrapolating thermodynamic descriptions of their corresponding binary and/or ternary systems. The extrapolation, although necessary, sometimes may cause some uncertainties in assessing thermodynamic parameters.

In TBCs, MCrAlY serves many crucial functions, such as providing oxidation resistance and bonding the ceramic top coat and substrate. Some physical properties of MCrAlY coatings exert an important role in determining the service life of TBCs, such as CTE. Among all the layers in TBCs, MCrAlY bond coats have the largest CTE. In order to alleviate the thermal expansion mismatch during service of TBCs, the most common approach is to reduce the CTE of MCrAlY bond coats [25]. The thermal expansion behavior of MCrAlY coatings is correlated to their compositions and phase constituents [26–28], and recently much attention has been paid to the influence of Re on the performance of MCrAlY coatings. Therefore, it is necessary to investigate the microstructural stabilities and performance of a NiCrAlY coating alloy containing Re. In this investigation, thermodynamic calculations of phase equilibrium were carried out using Thermocalc software package and utilizing TTNi7 database. The calculated phase constituents were compared with experimental results. It is worth noting that the TTNi7 database does not include element yttrium (Y), so that the presence of any possible Y-containing phases in the alloy could not be taken into account. Only Ni, Cr, Al, and Re elements as well as liquid, γ-Ni, γ'-Ni_3Al, β-NiAl, α-Cr, and σ-phases were chosen for the calculation. A more extensive description of calculation procedures can be found elsewhere [29].

Experimental approach

The alloy was prepared in an induction furnace using an alumina crucible and cast in a sand mold under an inert atmosphere, yielding a polycrystalline ingot with a nominal composition of Ni–22Cr–10Al–0.5Y–5Re (in wt%). Samples were cut from the ingot, ultrasonically cleaned in acetone, and then sealed in encapsulated quartz ampoules with a vacuum at 10^{-2} Pa to minimize oxidation. Heat treatments were subsequently carried out at temperatures between 700 and 1250 °C for 100 h in a laboratory furnace within an error of ±3 °C. Water quenching followed all treatments.

Microstructural characterization was carried out on the samples after thermal treatments. The thermally exposed samples were mechanically polished and electrolytically etched at 3 V with the reagent consisting of 24 mL H_2O + 42 mL H_3PO_4 + 34 mL H_2SO_4. Another reagent of 40 mL HCl + 8 mL HNO_3 was also used to reveal NiAl martensitic morphology. The etched samples were examined by SEM (JSM-6301F, JEOL Tokyo Japan) equipped with an energy dispersive X-ray spectroscope (EDS). Samples for TEM were electrochemically polished in a solution of 8 vol% perchloric acid and 92% ethanol at −20 °C. TEM observations were performed on a FEI TECNAIG2 20 microscope. The coefficient of thermal expansion (CTE) was measured using a UnithermTM-1252 ultra high temperature dilatometer with an error of <±5% between 200 and 500 °C and <±3% between 500 and 2500 °C. The heating rate was 3 C/min and the base temperature was 22 °C. Microhardness was measured on a Leco LM 247AT hardness tester with a load of 200 g and a dwell time of 13 s. A combination of TEM/SAED and X-ray diffraction (D/max_RA XRD) was used for identifying the phases present.

Results and discussion

Microstructural observations

The microstructure of the as-cast NiCrAlYRe alloy is shown in Fig. 1 where three main regions can be indentified (Fig. 1a). SEM/EDS results suggest that: one is associated with the β-NiAl phase with some α-Cr precipitates (Fig. 1b), another is a γ'-Ni_3Al/α-Cr region (Fig. 1c), and the other is the large blocky α-Cr grains most of which distribute along the boundaries of the other two regions. Typical XRD patterns of the thermally exposed specimens are presented in Fig. 2. According to the intensity and amount of XRD peaks, the phases of this alloy are temperature-dependent. It is found that γ'-Ni_3Al and β-NiAl only exist in a certain temperature range. When the temperature increases to 1000 °C, only a few peaks of γ-Ni, α-Cr, and martensite exist. This means that temperature increases result in phase changes in the alloy.

γ'-Ni_3Al/α-Cr region

The morphology of the γ'-Ni_3Al/α-Cr region evolves with increasing temperatures (Fig. 3). The rod-like and blocky α-Cr particles are found to precipitate within the γ'-Ni_3Al matrix in the sample quenched from 900 °C (Fig. 3a).

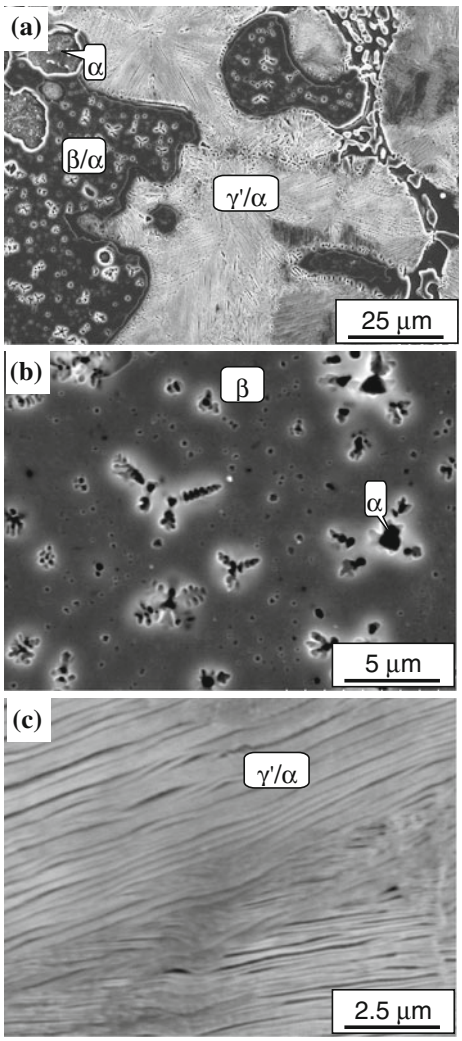

Fig. 1 **a** SEM micrograph of the as-cast NiCrAlYRe alloy, **b** higher magnification of the β-NiAl/α-Cr region, and **c** higher magnification of the γ'-Ni_3Al/α-Cr region

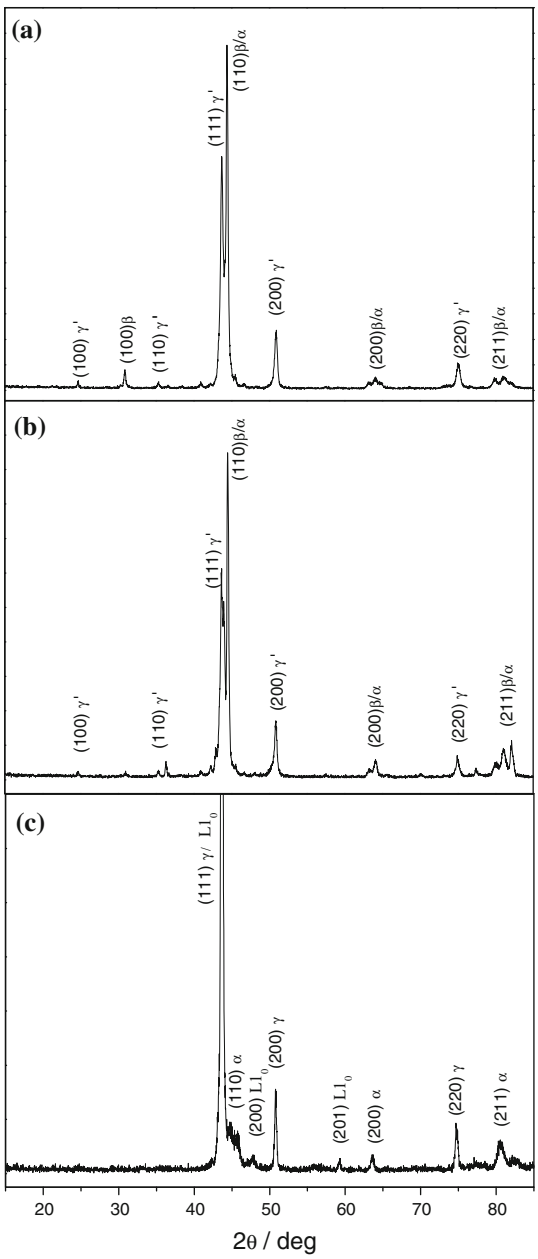

Fig. 2 XRD patterns of the specimens quenched from **a** 700 °C, **b** 900 °C, and **c** 1000 °C

When exposed to 1050 °C, the morphology and distribution of α-Cr precipitates becomes much more regular (Fig. 3b). When the quenching temperature is 1150 °C, the amount of α-Cr precipitates in this region reduces abruptly (Fig. 3c). It is worth noting that when the quenching temperatures are above 1000 °C, the γ'-Ni_3Al phase is replaced by γ-Ni. It is speculated that this phase transformation should be related to a four-phase reaction, γ'-Ni_3Al + α-Cr(Re) → γ-Ni(Cr,Re) + β-NiAl(Cr), which is mentioned in other articles [30, 31]. SEM/EDS results show that the concentration of Re is almost zero in γ'-Ni_3Al, and it is about 1 at.% in γ-Ni.

β-NiAl region

Figure 4 indicates that the amount of α-Cr particles in the β-NiAl matrix decreases gradually as temperature increases. When temperature is higher than 1150 °C, α-Cr present in the β-NiAl region dissolves. The morphology of the α-Cr particles changes from an initial dendrite-like morphology (Fig. 4a) to a spherical morphology (Fig. 4c) as exposure temperature rises. It is seen from Fig. 5 that there are some tiny particles as well as dendrite-like α-Cr particles precipitating within the β-NiAl. TEM/EDS results reveal these tiny particles are rich in Cr and Re, and they are thus presumed to be α-Cr. The tiny α-Cr particles probably precipitate during quenching.

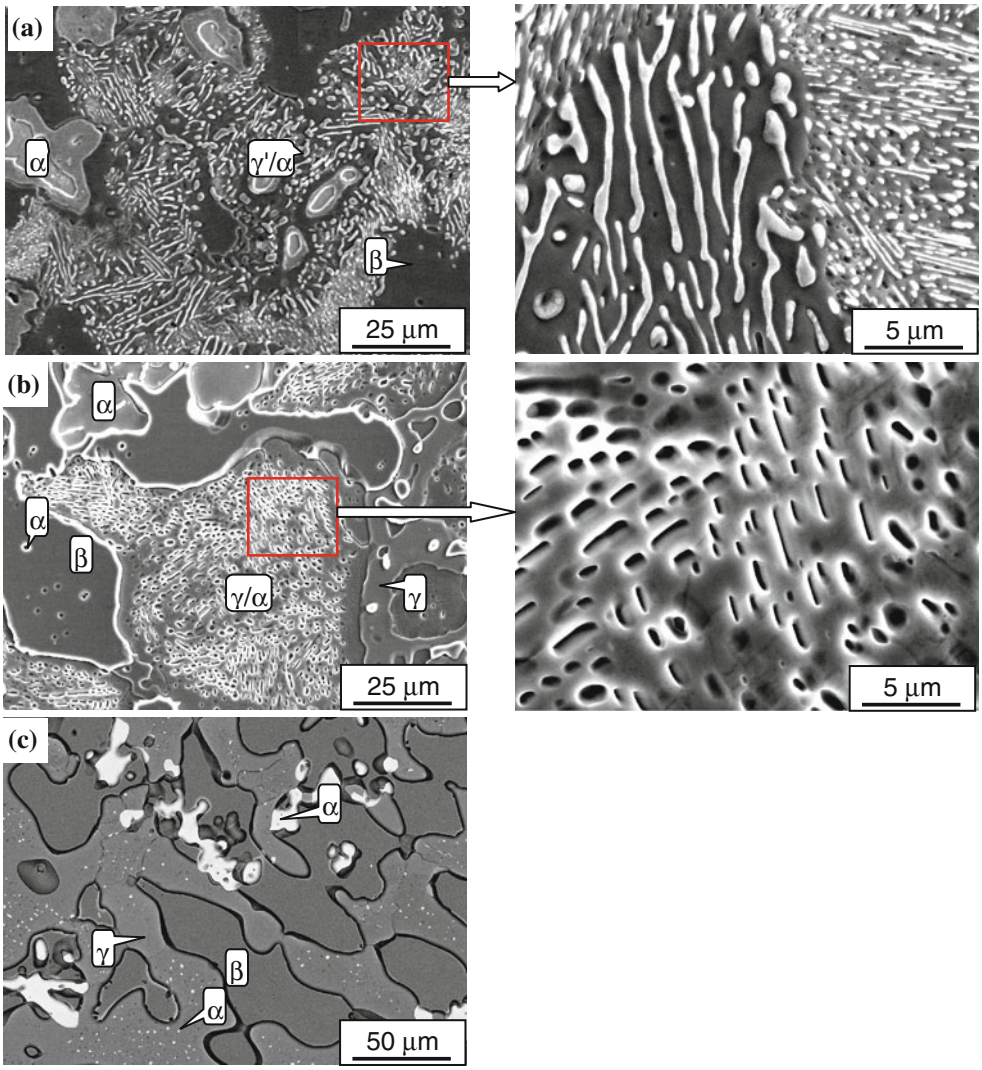

Fig. 3 SEM (**a** 900 °C, **b** 1050 °C) and BSE (**c** 1150 °C) micrographs of the γ'-Ni_3Al/α-Cr region in the samples quenched from different temperatures

All the samples were also etched by another reagent to reveal NiAl martensite, and it is found that in the samples quenched from temperatures higher than 1000 °C, the β-NiAl phase transforms from a body-centered-cubic (B2) structure to a face-centered-tetragonal (f.c.t.) $L1_0$ martensitic structure [32]. Figure 6 shows an etched view of the NiAl region after quenching from 1000 and 1100 °C. The characteristic striated structure of martensite is very visible. This microstructure is very similar to that observed in NiAl bond coats [5]. In some individual grains the martensitic plates show different orientations.

Quantitative SEM/EDS results (Table 1) reveal that the concentration of Cr in the NiAl phase increases from approximately 4.4 at.% at 700 °C to 11.7 at.% at 1250 °C, but little Re is detected in this phase within the accuracy of the EDS. It should be noted that the $x_{(Al+Cr)}$ to $x_{(Ni)}$ ratios (x denotes the mole fraction) in the NiAl phase remain almost unchanged in all specimens (~42:58). This phenomenon can be explained by the fact that Cr shows a site preference for the Al sublattice in the Ni-rich β-NiAl phase [33, 34]. It is reported that binary NiAl phase containing more than 63 at.% Ni will undergo a martensitic transformation when quenched from temperatures higher than 1000 °C [3–7], but the concentration of Ni in the NiAl phase in the studied alloy is lower than 60 at.%. So it is suggested that the solid solution of Cr may influence the martensitic transformation behavior of the NiAl phase.

Blocky α-Cr grains

The large α-Cr grains experience Ostwald ripening, increasing the size of the α-Cr grains (Fig. 7). According to SEM/EDS results, the distribution of alloying element Re in the α-Cr grains is nonuniform in the samples exposed to

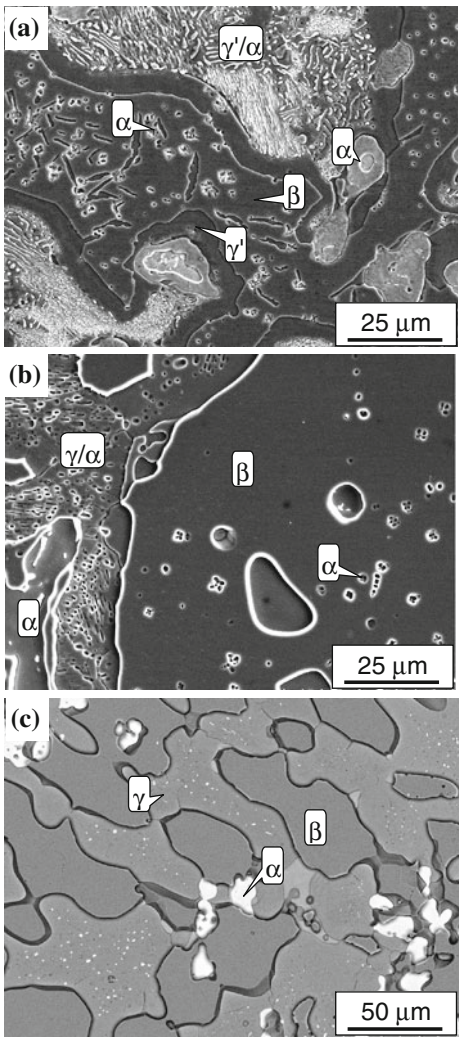

Fig. 4 SEM (**a** 900 °C, **b** 1050 °C) and BSE (**c** 1150 °C) micrographs of the β-NiAl/α-Cr region in the samples quenched from different temperatures

temperatures below 900 °C. Re is much richer in the center of the α-Cr grains. The nonuniform distribution of Re in α-Cr may be inherent to the solidification process. The exposure time (100 h) is not long enough for Re atoms to diffuse sufficiently since diffusion of Re atoms is very slow below 900 °C. In the specimens exposed to higher temperatures, the concentration of Re in α-Cr becomes uniform, and increases from about 18 at.% at 1000 °C to about 26 at.% at 1250°C.

Y-rich intermetallic

Y-rich intermetallic is found along β and/or γ grain boundaries (Fig. 8). This intermetallic was identified as Ni_5Y in our previous work [35]. Nash et al. [36] reported that the alloying element, Al, has a substantial solubility in Ni_5Y; thus this intermetallic is also described as

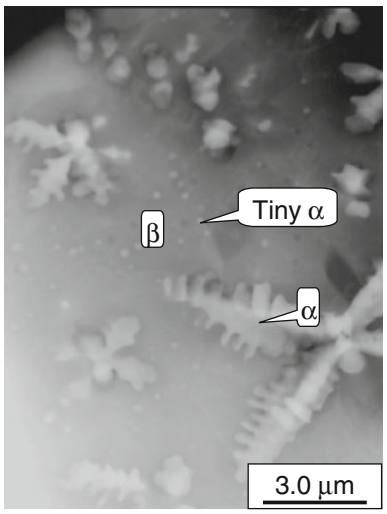

Fig. 5 Bright-field TEM micrograph of β-NiAl/α-Cr region in the sample quenched from 800 °C

$Al_xNi_{5-x}Y$. In this study, the alloying element Cr is also present in this intermetallic in solid solution as much as 12.2 at.%. The composition of the Y-rich particle (61.4Ni–12.2Cr–18.0Al–8.4Y in at.%) is almost independent of temperature according to EDS results.

The observation outlined above illustrates that the NiCrAlYRe coating alloy is mainly composed of β-NiAl, γ-Ni, γ'-Ni_3Al, α-Cr, and NiAl martensite phases. In the samples exposed to temperatures below 900 °C, the main phases are γ'-Ni_3Al, α-Cr, and β-NiAl; as temperature rises, the phase constituent is changed to be γ-Ni, α-Cr, and NiAl martensite.

Thermodynamic calculation

Figure 9 shows the calculated isothermal sections of the ternary NiCrAl system with and without Re. The addition of 5 wt% Re causes the $\alpha + \beta \rightarrow \beta$ equilibrium line to shift toward lower Cr concentrations. This indicates a lower solubility of Cr and a higher Ni in β. Re also expands the $\alpha + \beta + \gamma$ phase region at the expense of the $\beta + \gamma$ phase region. In addition, the $\beta + \gamma'$ and γ' phase regions shrink toward lower Cr concentration. This is due to a decreased solubility of Cr in both γ' and β. It is suggested that Re promoting the amount of α is probably caused by a decreased solubility of Cr in γ' and β.

The phase constituents in the studied NiCrAlYRe coating alloys have been calculated in the temperature range from 600 to 1400 °C, and the results are presented in Fig. 10. The alloy consists of α, β, and γ' at temperatures below 1000 °C, and then experiences a four-phase reaction ($\alpha + \gamma' \rightarrow \beta + \gamma$) [30, 31]. This reaction causes an obvious change in the amounts of the involved phase: γ' disappears and γ is observed. This calculated phase

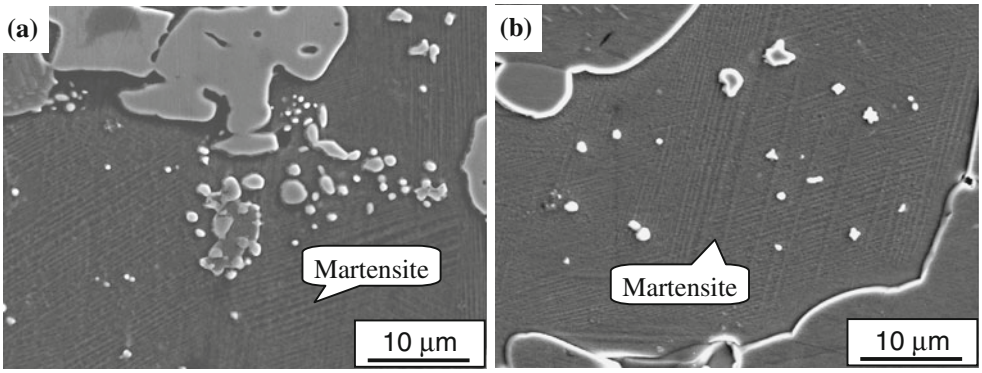

Fig. 6 SEM micrographs of NiAl martensite in the samples quenched from different temperatures (**a** 1000 °C, **b** 1100 °C)

Table 1 Average concentrations of elements in NiAl phase after quenched from different temperatures (at.%)

Temperature (°C)	700	900	1000	1100	1200	1250
Ni	56.6	57.7	58.8	58.4	58.2	58.5
Al	39.0	36.4	33.4	32.5	30.3	29.8
Cr	4.4	5.9	7.8	9.1	11.5	11.7

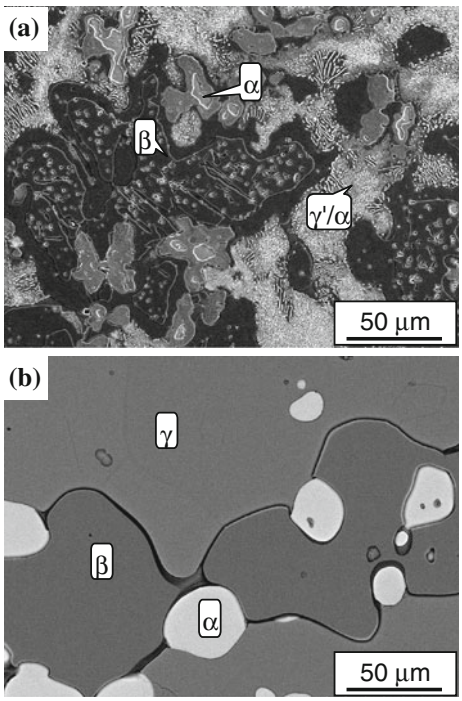

Fig. 7 SEM (**a** 900 °C) and BSE (**b** 1250 °C) micrographs of α-Cr in the sample quenched from different temperatures

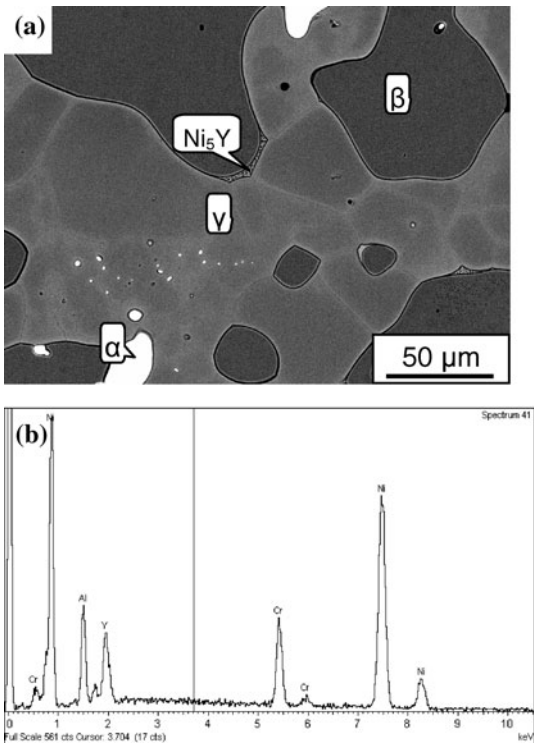

Fig. 8 **a** BSE micrograph of Y-rich precipitate in the sample quenched from 1200 °C and **b** the corresponding EDS result

transformation (Fig. 10) agrees reasonably well with the experimentally observed phase evolution associated with temperatures (Fig. 3) mentioned in "Microstructural observations" except for the transformation temeprature. Experimental results reveal that the transformation occurs between 900 and 1000 °C, while the thermodynamic calculations show that it takes place between 1000 and 1050 °C. The discrepancy between the two results may be associated with the following reasons. First, for ternary and higher order systems, the thermodynamic parameters of these systems are obtained by extrapolation of the thermodynamic descriptions of their lower order systems; this extrapolation may introduce considerable uncertainty. Secondly, the TTNi7 database is designed based on experimental data obtained from typical Ni-base superalloys, and applied for predicting the equilibria of superalloys, such as the γ/γ', γ' solvus, and solidus/liquidus relations. However, the investigated Ni–22Cr–10Al–0.5Y–5Re alloy contains much more Cr and Al than typical

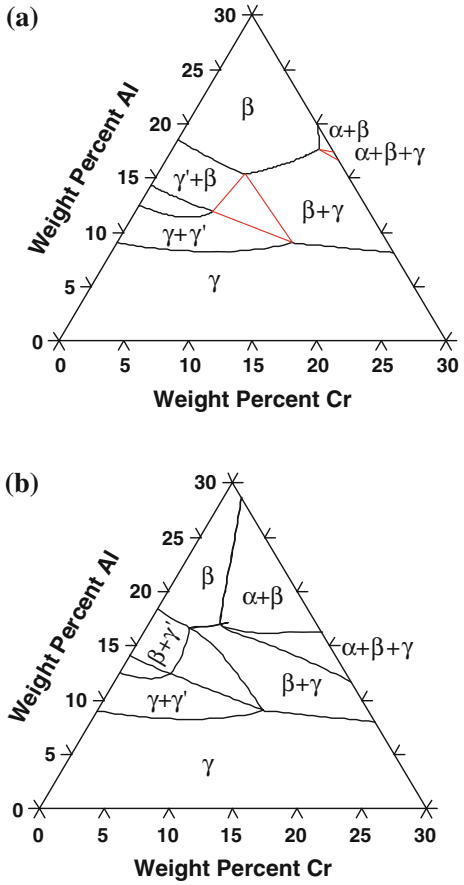

Fig. 9 Calculated isothermal diagrams of **a** NiCrAl and **b** NiCrAl-5Re systems at 1200 °C

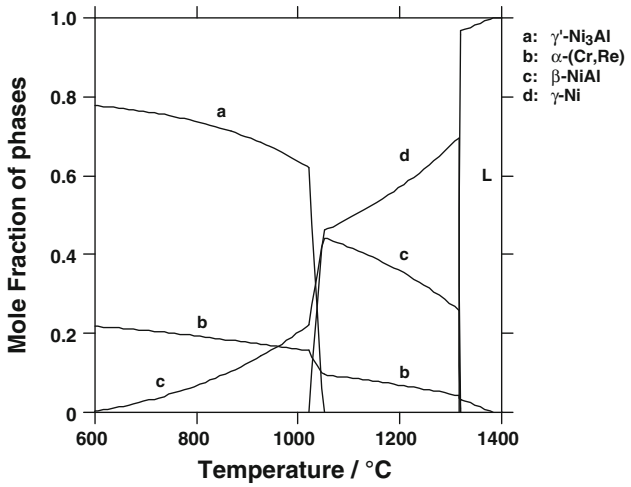

Fig. 10 Calculated phase fractions in the studied alloy

superalloys. This also may lead to some deviation. The time of thermal exposure in this investigation is not long enough for the atoms in the alloy to diffuse sufficiently to reach thermodynamic equilibrium, especially for temperatures lower than 1000 °C. It is worth noting that TTNi7

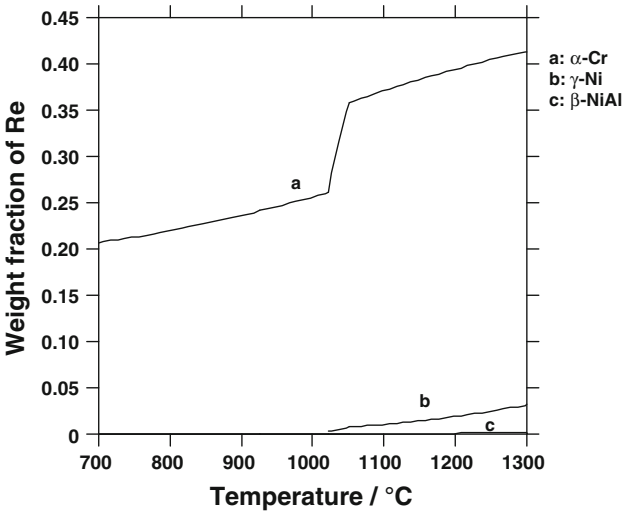

Fig. 11 Calculated weight fractions of Re in α, γ, and β-phases in the studied alloy

database does not include the minor alloying element Y, so the presence of any possible Y-containing phases in the alloy could not be taken into account during thermodynamic calculations.

Figure 11 shows the weight fractions of Re in all the phases. According to the figure, Re partitions exclusively into the α-Cr phase, and is hardly found in both the γ'-Ni_3Al and the β-NiAl phases. The phase diagrams [21] of the Ni–Re, Al–Re, and NiAl–Re systems also suggest that Re has very limited solid solubility in the γ'-Ni_3Al and the β-NiAl phases. This may be because the interaction between Re and Al atoms is repulsive while the interaction between Re and Cr is attractive, so Re can partition easily into the α-Cr phase, while has little solubility in Al-rich γ'-Ni_3Al and β-NiAl.

Although there are some discrepancies between the calculated and the experimental results, such as the value for the dissolution temperature of γ' and the existence of Ni_5Y intermetallic, the TTNi7 database is still useful when predicting the phase stabilities of MCrAlY coatings when there is no thermodynamic database available for MCrAlY coatings now.

CTE

The failure of TBCs is mainly influenced by the stress distribution in TBC systems. In thermal cycling conditions, stresses can be generated in the Al_2O_3 scale due to CTE mismatch between coating layers. If the generated stresses cannot be relieved by time-dependent creep processes, once the strain energy in the coating reaches the fracture energy of the metal–scale interface, cracking and spallation of the scale might occur. Hence, in addition to oxidation resistance, CTE and mechanical properties of MCrAlY

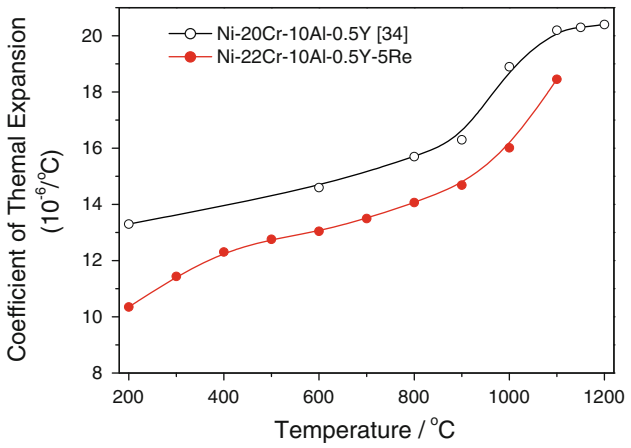

Fig. 12 Coefficients of thermal expansion of the studied NiCrAlYRe alloy and a NiCrAlY alloy

coating alloys also play an important role in determining the service life of MCrAlY coatings and TBCs.

Figure 12 shows the CTE data for NiCrAlYRe and NiCrAlY alloys. The similarity in the shape of the two curves implies that the thermal expansion behavior of the two alloys is similar. The CTE of the Ni–20Cr–10Al–0.5Y (http://www.ms.ornl.gov/researchgroups/corrosion/publications/pintpub/pub15.pdf) alloy changes linearly with temperature below 900 °C, followed by a sudden rise; the CTE of the studied alloy increases gradually with temperatures until 1000 °C, also followed by a notable rise. Merchant and Notis [37] reported that an increase in the slope of the CTE of the Ni–20Cr–10Al–0.5Y alloy from 900 to 1050 °C was probably caused by the phase transformation of γ'-Ni_3Al + α-Cr(Re) → γ-Ni(Cr,Re) + β-NiAl(Cr). Combining Merchant's conclusion with our microstructure observation results, it is predicted that the evident increase in the CTE of the studied alloy from 900 to 1050 °C is a result of the phase transformation: γ'-Ni_3Al + α-Cr(Re) → γ-Ni(Cr,Re) + β-NiAl(Cr).

In addition, the CTE of the NiCrAlYRe alloy is apparently lower than that of the Ni–20Cr–10Al–0.5Y alloy. This may be related to the addition of Re. Phillips and Gleeson [38] reported that the presentation of α-Cr at the alloy/scale interface decreased the scale spallation by providing a lower CTE mismatch between the alloy and the Al_2O_3-rich scale. It is seen in Table 2 that α-Cr has a CTE lower than γ-Ni and β-NiAl. Therefore, an increase in the amount of Re-rich α-Cr should result in a decrease in CTE.

Microhardness

The microhardness data shown in Table 3 are averages of six data points with an error of ±10 Hv. The microhardness of the γ'-Ni_3Al/α-Cr and γ-Ni/α-Cr regions decreases with increasing exposure temperatures. The microhardness of the

Table 2 Physical thermal expansion values for α-Cr, γ-Ni, γ'-Ni_3Al, β-NiAl, and Al_2O_3 phases from room temperature to 1000 °C

Phases	α-Cr	γ-Ni	γ'-Ni_3Al	β-NiAl	Al_2O_3
CTE	9.6	19.8	16.7	16.3	9.7

Table 3 Average microhardness of the regions of β-NiAl/α-Cr, γ'-Ni_3Al/α-Cr, and γ-Ni/α-Cr in the samples quenched from different temperatures

Temperature (°C)	700	800	900	1000	1050	1100	1150	1200	1250
β-NiAl/α-Cr	483	428	366	548	534	487	485	584	548
γ'-Ni_3Al/α-Cr	555	478	426	407					
γ-Ni/α-Cr					347	302	306	285	284

β-NiAl/α-Cr region goes down from 483 Hv at 700 °C to 366 Hv at 900 °C, and it is supposed to decrease continually. However, for the samples quenched from temperatures above 1000 °C, the microhardness of this region is higher than that from 900 °C. As for the blocky α-Cr region, it is impossible to identify its specific microhardness because the size of the α-Cr grain is too small to measure.

The microhardness of the β-NiAl/α-Cr region in the specimen quenched from temperatures above 1000 °C is higher than those from 900 °C. The concentration change of this phase may not be responsible for the obvious increase in microhardness, because the concentrations of all elements in the β-NiAl are almost the same in the specimen exposed to the temperature from 900 to 1000 °C. Also, the dissolution behavior of partial α-Cr precipitates in the β-NiAl phase cannot cause such a sharp rise since the microhardness of the α-Cr phase is much higher than β-NiAl, and its dissolution should reduce the hardness. So there must be some intrinsic microstructure or crystallographic change in the β-NiAl phase. The microstructural observation reveals that the β-NiAl undergoes martensitic transformation when quenched from temperatures higher than 1000 °C, it is concluded that the martensitic transformation causes an increase in the microhardness of the β-NiAl phase. This martensitic transformation probably also influences other mechanical properties that can affect the service lifetime of coatings. From Table 3, it is also seen that the microhardness increases apparently from 1150 to 1200 °C. This phenomenon is probably related to the temperature dependence of the microstructure of NiAl martensite, which needs further investigation.

Conclusions

The phase constituents and properties, such as thermal expansion and microhardness of the NiCrAlY coating alloy

with Re addition, were investigated in the temperature range from 700 to 1250 °C. In the samples quenched from temperatures below 900 °C, the main phases were γ'-Ni_3Al, α-Cr and β-NiAl. As temperature goes up, the phases present change to be γ-Ni, α-Cr, and NiAl martensite. Martensitic transformation of B2 β-NiAl phase occurred when quenching from temperatures higher than 1000 °C, and had an important influence on the microhardness of this phase. The addition of Re promoted the formation of Cr-rich α-phase, thereby decreasing the CTE of the NiCrAlYRe coating alloy.

Acknowledgements This study was financially supported by the National Basic Research Program (973 Program) of China under Grant No. 2010CB631200 (2010CB631206) and the National Natural Science Foundation of China (NSFC) under Grant No. 50931004 and 51071164.

References

1. Shankar S, Koenig DE, Dardi LE (1981) J Met 33:13
2. Daleo JA, Ellison KA, Boone DH (2002) J Eng Gas Turbine Powder 124:571
3. Chen MW, Livi KJT, Wright PK, Hemker KJ (2003) Metall Mater Trans 34A:2289
4. Hemker KJ, Mendis BG, Eberl C (2008) Mater Sci Eng A 483:727
5. Zhang Y, Haynes JA, Pint BA, Wright IG, Lee WY (2003) Surf Coat Technol 163–164:19
6. Mendis BG, Tryon B, Pollock TM, Hemker KJ (2006) Surf Coat Technol 201:3918
7. Rosen S, Goebel JA (1968) Trans Metall Soc AIME 242:722
8. Chen MW, Ott RT, Hufnagel TC, Wright PK, Hemker KJ (2003) Surf Coat Technol 163–164:25
9. Chen MW, Glynn ML, Ott RT, Hufnagel TC, Hemker KJ (2003) Acta Mater 51:4279
10. Pan D, Chen MW, Wright PK, Hemker KJ (2003) Acta Mater 51:2205
11. Mendis BG, Hemker KJ (2008) Scripta Mater 58:255
12. Czech N, Schmitz F, Stamm W (1995) Surf Coat Technol 76–77:28
13. Baufeld B, Bartsch M, Brož P, Schmücker M (2004) Mater Sci Eng 384A:162
14. Baufeld B, Schmücker M (2005) Surf Coat Technol 199:49
15. Beele W, Czech N, Quadakkers WJ, Stamm W (1997) Surf Coat Technol 94–95:41
16. Achar DRG, Munoz-Arroyo R, Singheiser L, Quadakkers WJ (2004) J Phys IV France 120:231
17. Achar DRG, Munoz-Arroyo R, Singheiser L, Quadakkers WJ (2004) Surf Coat Technol 187:272
18. Täck U (2004) The influence of cobalt and rhenium on the behavior of MCrAlY coatings. Ph.D. dissertation, Tech. Univ. Freiberg
19. Huang W, Chang YA (1998) Intermetallics 6:487
20. Huang W, Chang YA (1999) Intermetallics 7:863
21. Huang W, Chang YA (1999) Mater Sci Eng A259:110
22. Huang W, Chang YA (1998) J Alloy Compd 274:209
23. Ansara I, Dupin N, Lukas HL, Sundman B (1997) J Alloy Compd 247:20
24. Dupin N, Ansara I, Sundman B (2001) Calphad 25:279
25. Hasselman DPH, Johnson LF, Bentsen LD, Syed R, Lee HL, Swain MV (1987) Am Ceram Soc Bull 66:799
26. Taylor TA, Walsh PN (2004) Surf Coat Technol 188–189:41
27. Taylor TA, Walsh PN (2004) Surf Coat Technol 177–178:24
28. Taylor T, Foster J (2006) Surf Coat Technol 201:3819
29. Saunders N (2000) Ni-Data information. Thermotech, Surrey Technology Center, Surrey
30. Engström A (1996) Long-range diffusion and microstructural evolution in multiphase alloys—a combined thermodynamic and kinetic approach (PhD Thesis), Division of Physical Metallurgy, Department of Materials Science and Engineering, Royal Institute of Technology, Stockholm
31. Nijdam TJ, Kwakernaak C, Sloof WG (2006) Metall Mater Trans A 37:683
32. Tanner LE, Pelton AR, VanTendeloo G, Schryvers D, Wall ME (1990) Scripta Matall. Mater. 24:1731
33. Jiang C (2007) Acta Mater 55:4799
34. Frommeyer G, Fischer R, Deges J, Rablbauer R, Schneider A (2004) Ultramicroscopy 101:139
35. Liang JJ, Wei H, Hou GC, Zheng Q, Sun XF, Guan HR, Hu ZQ (2008) J Mater Res 23:2264
36. Nash P, Su HN, Kleppa O (2002) Trans Nonferrous Met Soc China 12:754
37. Merchant SM, Notis MR (1984) Sci Eng 66:47
38. Phillips MA, Gleeson B (1998) Oxid Met 50:399